Robust Chipless RFID Detection Using Complex Natural Frequency Along With the *k*-Nearest Neighbor Algorithm

FEAVEYA KHEAWPRAE, (Member, IEEE), **AKKARAT BOONPOONGA**, (Member, IEEE), **AND PRAYOOT AKKARAEKTHALIN**, (Member, IEEE)

Research Center of Innovation Digital and Electromagnetic Technology, Department of Electrical and Computer Engineering, Faculty of Engineering, King Mongkut's University of Technology North Bangkok, Bangkok 10800, Thailand

Corresponding author: Akkarat Boonpoonga (akkarat.b@eng.kmutnb.ac.th)

ABSTRACT This paper proposes a detection technique for the chipless RFID system. In the proposed technique, the experiments for measuring the scattering responses of all possible tags were conducted first in a free-space anechoic chamber in order to avoid the effect of unwanted signals due to the environment. The responses of all possible tags were exploited in order to extract poles, including natural frequencies and damping factors, by using the short-time matrix pencil method. All extracted poles successively chosen from the late-time portions were exploited to create the decision boundary by using the *k*-nearest neighbor algorithm. In order to validate the robustness of the proposed detection technique, experiments with the chipless RFID system with tags attached to containers, i.e. parcel and plastic boxes, were conducted. Poles extracted from the response of the tag attached to a container were fed to the decision boundary for ID detection. The poles that had fallen into the region labeled as logic "1" were detected as logic "1," and *vice versa*. The experiment results showed that the attachment of the tags to the containers caused a change in the poles. The conventional technique using only natural frequencies has exhibited poor performance regarding tag ID detection. On the other hand, the proposed detection technique achieved a 100% detection rate, although the extracted poles used to detect the bit logic were disturbed by the container. The experimental results confirm the superiority of the proposed system over conventional chipless RFID detection. Moreover, the proposed technique can be considered a robust detection technique.

INDEX TERMS Chipless RFID, detection, identification, short-time matrix pencil method, pole, *k*-nearest neighbor.

I. INTRODUCTION

Chipless radio frequency identification (RFID) technology has received considerable interest as a promising solution for many applications in sensing and tracking, such as sensors for structural health monitoring, tracking of inventory in retail settings, and smart packaging. This is because of its main advantage of not requiring silicon integrated circuits (ICs) or chips. The cost of the chipless RFID tags therefore has become lower than that of the conventional tags equipped with ICs. The basic principle of operation of the chipless

RFID system is similar to that of the radar target identification system. The reader of the system transmits a wideband signal to a tag, and the signal backscattered from the tag is then measured and analyzed in the time and/or frequency domains in order to retrieve the desired information. The chipless RFID technology can be broadly classified into two main categories—namely, time-domain reflectometry (TDR)-based chipless RFID and frequency-signature-based chipless RFID.

With the TDR-based chipless RFID, a short pulse is transmitted from the reader to a tag and a train of the pulse reflected from the tag is created in order to decode the tag's data. There have been many attempts to propose a chipless

---

The associate editor coordinating the review of this manuscript and approving it for publication was Renato Ferrero.

RFID tag using TDR-based technology for data encoding. One of the most commercially available chipless RFID tags is based on the surface acoustic wave (SAW) structure. The main advantage of the SAW-based tag is its robustness regarding environmental effects. In contrast, there is the main drawback of its complex structure; it is more expensive than the conventional tags equipped with ICs and is non-printable on paper or plastic-based items [1], [2]. The chipless RFID tag based on the meandering delay transmission line using microstrip technology was proposed to generate the tag identification (ID) [3], [4]. In [5], the delay line structure was designed for the chipless RFID permittivity sensor. Although the proposed tags use a replica of the SAW-based tag, the microstrip technology makes it printable. A comparative survey of the SAW-based and silicon-based tag was presented [6]. The article provided many studies on reader technologies, the performance of many metrics, the deploy potential, etc. However, the chipless RFID tag was not taken into account in this survey article.

Another chipless RFID technology is based on the frequency spectrum signature. The basic principle of the frequency-based chipless RFID tag is to use its spectral response to encode information. The tag structure is designed to control the desirable specific amplitude and/or phase characteristics over the frequency range of interest. A planar microwave circuit has been widely used to design a tag and to encode the data information with the presence or absence of a resonant peak in the amplitude or phase spectra [7]. For example, a chipless RFID tag was designed on the coplanar waveguide utilizing two cross polarized ultra-wideband (UWB) antennas for transmission and reception. Multiple stopband spiral resonators were placed between antennas in order to encode the 23-bit data information in the frequency range of 5 GHz to 10.7 GHz [8]. In [9], the chipless RFID tag consisting of multiple resonators and two cross-polarized ultra-wide band antennas was proposed. The resonance frequency of the proposed tag can be adjusted by an isolated leg of the U-shaped microstrip-based resonators. Another frequency-based chipless RFID tag was proposed in [10] in which the number of resonators was maximized in a limited space, while the frequency separation between the resonators was minimized. Note that these approaches generate the tag IDs by using present and/or absent resonant peaks.

The main limitation of the frequency-based chipless RFID technology is the bandwidth required in order to increase the information capacity. If the bandwidth is fixed, the adjacent notch or peak of the resonant frequencies identified as the bit logic will be closer to each other. The detection for the bit logic has become a serious problem. In order to overcome this problem, a two-dimensional frequency domain in terms of complex natural resonance (CNR) can increase the resolution of the detection while keeping the same bandwidth. A tag embedded with singularity has been proposed [11]. In this approach, the principle of the singularity expansion method (SEM) was applied to encode the tag ID into the tag's structure with the CNR, generally called the pole, and

to retrieve the tag ID from the late-time portion of the tag response by using the matrix pencil method (MPM). The main drawback of the MPM is that is requires prior knowledge of the commencement of the late time, which relies upon the geometry and orientation of objects [12], [13]. However, this knowledge is unknown for the non-cooperative scenario. In [14], the short-time matrix pencil method (STMPM) was proposed and experimentally demonstrated to extract poles embedded in the chipless RFID tag. The STMPM was slightly modified from the MPM by sliding the time windows by step times in order to mainly distinguish the late-time portion from the whole response. The STMPM was not only applied to the chipless RFID applications, but also to the radar target identification, as we proposed in [12], [13], [15]-[17]. In [18], the design and implementation of the high-density chipless RFID tag was proposed by using the basic principle of the SEM. Poles extracted by using the STMPM were employed as encoded data of the tag, corresponding to the variance in the design parameter of the tag. The encoded high-density data result in sensitivity to noise and unwanted effects due to the environment. Nevertheless, it has clearly shown that only the natural frequency rather than poles was employed to represent the tag ID. In addition, although these approaches have employed poles extracted by using the MPM or STMPM to represent the data encoded in the chipless RFID tag, they have not realized the necessity of the detection technique for tag identification. In order to detect the bit logic of the frequency-based tag, simple techniques such as the Euclidean distance calculated from the adjacent frequency notch or peak have been widely used [19], [20]. The notch or peak will be closer when the number of bits is increased. This implies that this detection will be sensitive to the noise and unwanted effects resulting in a change in the frequency notch or peak.

This paper therefore extends and validates the use of poles to represent the tag ID and introduces the detection technique using the k-nearest neighbor (k-NN) algorithm. This algorithm, one of the most popular non-parametric classifications, has been widely used with many applications such as online handwritten signature detection [21], the classification of big data in healthcare [22], and pattern recognition in cloud chipless RFID processing [23]. Because of the non-parametric classification, the algorithm does not require prior knowledge of the probability distributions of the samples in the classification problem. Moreover, it is not only simple, but its performance also relies only on parameter k. One of the interesting applications of the RFID system using the k-NN algorithm is the location tracking. In [24] the k-NN algorithm was slightly modified as an adaptive k-NN in order to estimate the location of the tracing tag. In this paper, poles extracted from the responses of all possible tags measured in a free-space anechoic chamber are exploited in order to create the decision boundary first by using a k-NN algorithm. The created decision boundary is larger than the detection frequency range obtained from the use of only the natural frequency or RCS spectra.
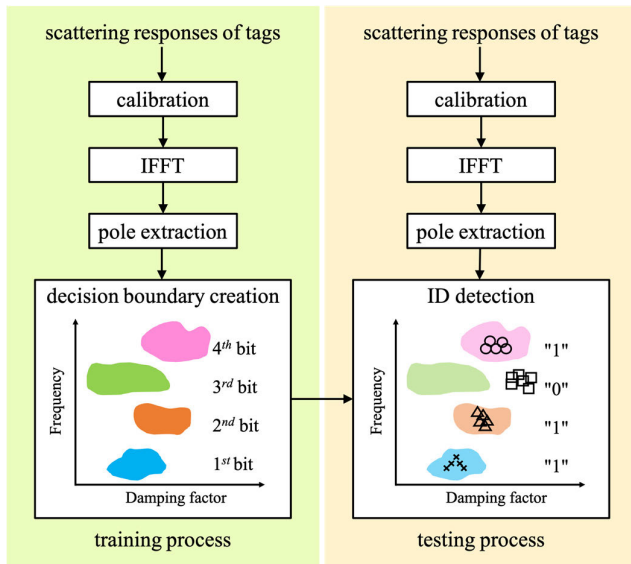
FIGURE 1. Process diagram of the proposed chipless RFID detection.

FIGURE 2. Basic diagram of the chipless RFID system based on the SFCW with a bistatic configuration.

The contributions of this paper are as follows. First, the bit logics of the chipless RFID tag are represented by using poles that are in the two-dimensional frequency domain. This results in the change of detection of the bit logic of the chipless RFID tag from the frequency range to the area of complex natural frequencies. Second, the k-NN algorithm was applied to create the decision boundary employed for detecting the bit logic of the chipless RFID tag. Third, the effect of the container on the detection performance of the chipless RFID system using the poles along with the k-NN algorithm was investigated by experiments. This paper is organized as follows. After the introduction, the basic principle of the proposed technique is presented in Section II where calibration is also introduced in order to mitigate unwanted effects. In Section III, the creation of the decision boundary is discussed. All possible tags particularly designed for being attached to the container are measured in order to create the decision boundary. In Section IV, experiments with the proposed chipless RFID system were conducted in order to validate the detection performance. The effect of the container on the extracted poles and detection performance was taken into account. Finally, conclusions are drawn in Section V.

II. PROPOSED TECHNIQUE
In this section, a technique for chipless RFID detection is proposed and described along with its associated equations. In the proposed technique, calibration is introduced in order to mitigate the unwanted effects caused by the antenna response and surrounding environment. A pole extracted from the tag response in the time domain by using the STMPM is exploited as a tool rather than only frequency in order to detect the bit logic of the tags. Fig. 1 is a process diagram of the proposed technique. The process was divided into two main categories: training and testing processes.
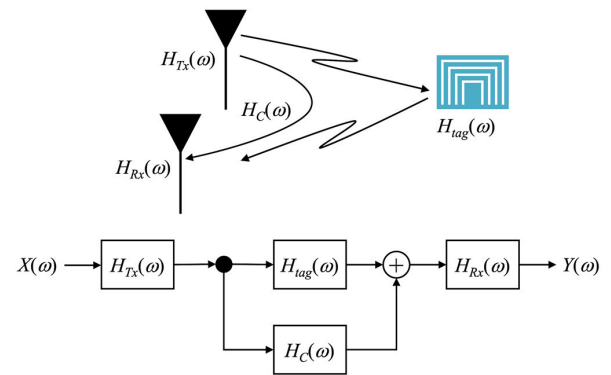
In the training process, the scattering coefficient S_{21} of all possible tags used as references was measured in a free-space anechoic chamber. The calibration was conducted in the frequency domain in order to mitigate the unwanted effects and the inverse Fourier transform was then used to transform the resulting frequency-domain response to the time-domain response. Poles, including natural frequencies and damping factors, were extracted from the time-domain response by using the STMPM. Some of the successive extracted poles of all the possible tags were chosen from the late time in order to create the decision boundary by using the k-NN algorithm. The decision boundary obtained from the training process by using the k-NN algorithm is a tool of the proposed chipless RFID system in order to detect the bit logic of tags. In the testing process, the tag that needs to be determined is measured in practical situations, such as installation to the container. The signal processing processes, i.e. calibration, inverse Fourier transform, and pole extraction, were re-performed, as shown in Fig. 1. The tag's poles obtained from the extraction process using STMPM were fed to the detection process by putting them into the pre-created decision boundary to determine the logic of the tag. If the extracted poles of the tag are in the region predefined as logic "1," they are detected as logic "1," and vice versa. Next, the principle of the signal processing in the proposed technique is discussed.

A. CALIBRATION
The basic diagram of the chipless RFID system based on stepped-frequency continuous wave radar (SFCW) with a bistatic configuration is shown in Fig. 2. The signals with the swept frequencies are transmitted by using a transmitting antenna to a chipless RFID tag and the backscattering signals are then received by using the receiving antenna. In order to mitigate the unwanted effects caused by the unflat antenna response and surrounding environments, calibration is introduced [15], [16]. According to Fig. 2, the total transfer function of the chipless RFID system can be expressed as

$$H_{total}(\omega) = H_{Tx}(\omega)H_{tag}(\omega)H_{Rx}(\omega)$$
$$+H_{Tx}(\omega)H_c(\omega)H_{Rx}(\omega) \qquad (1)$$

where $H_{Tx}(\omega)$ and $H_{Rx}(\omega)$ denote the transfer functions of the transmitting and receiving antennas, respectively. The transfer function of the chipless RFID tag, and mutual coupling between the antennas, are denoted by $H_{tag}(\omega)$ and $H_c(\omega)$, respectively. Note that the right-hand-side term in (1) represents the context of the measurement in the free space without a tag and then is given by

$$H_{no\ tag}(\omega) = H_{Tx}(\omega)H_c(\omega)H_{Rx}(\omega). \tag{2}$$

The (1) and (2) are then rearranged and given by

$$H_{total}(\omega) - H_{no\ tag}(\omega) = H_{Tx}(\omega)H_{tag}(\omega)H_{Rx}(\omega). \tag{3}$$

The aim of performing the calibration is to achieve the pure transfer function of the tag $H_{tag}(\omega)$. However, the $H_{Tx}(\omega)$ and $H_{Rx}(\omega)$ are still in (3). The reference transfer function $H_{plate}(\omega)$ is therefore required. A large metal plate is placed instead of the tag. Since the plate is assumed to be a perfect reflector for all frequency bands, its transfer function is equal to -1. Thus, the reference transfer function and -1 are respectively substituted into the total transfer function $H_{total}(\omega)$ and transfer function of the tag $H_{tag}(\omega)$ as given by

$$H_{plate}(\omega) - H_{no\ tag}(\omega) = -H_{Tx}(\omega)H_{Rx}(\omega). \tag{4}$$

Hence, the transfer function of only the tag can be expressed by

$$H_{tag}(\omega) = \frac{H_{total}(\omega) - H_{no\ tag}(\omega)}{H_{plate}(\omega) - H_{no\ tag}(\omega)}. \tag{5}$$

B. POLE EXTRACTION USING STMPM

In order to extract the poles by using the STMPM, the transfer function of the tag, obtained after performing calibration, must first be inversed to the tag's time-domain response expressed as

$$h_{tag}(t) = \mathcal{F}^{-1}\{H_{tag}(\omega)\} = y_e(t) + y_l(t) + \eta(t) \tag{6}$$

where $y_e(t)$, $y_l(t)$, and $\eta(t)$ represent the early-time response, late-time response, and additive noise, respectively. Based on the SEM principle, the late-time response of the chipless RFID tag can be modeled as a sum of the damped exponentials with complex natural frequencies as follows

$$y_l(t) = \sum_{i=1}^{M} R_i^T e^{s_i t} + \eta(t) \tag{7}$$

where $s_i = \sigma_i + j\omega_i$ denotes the ith pole, which is the complex frequency comprising damping factor σ_i and angular natural frequency ω_i. The R_i denotes the complex residue, while M is the number of poles. Regarding the method of pole extraction, the MPM first proposed in [25] was slightly modified by moving the appropriate time window along the entire time-domain response. The modified MPM is referred to as the STMPM [14]. Based on the STMPM, the time window with a length of T_w is slightly moved along the time

axis incrementally by T. The windowed late-time response can be written as

$$y_l^T(t) = \sum_{i=1}^{M} R_i^T e^{s_i(t-T)} \tag{8}$$

in which

$$R_i^T = R_i e^{s_i T} = R_i e^{(\sigma_i + j\omega_i)T}. \tag{9}$$

For each windowed time-domain response, the poles are extracted by beginning to form the matrix $[Y_l^T]$ given by

$$[Y_l^T] = \begin{bmatrix} y_l^T(0) & y_l^T(1) & \cdots & y_l^T(L) \\ y_l^T(1) & y_l^T(2) & \cdots & y_l^T(L+1) \\ \vdots & \vdots & \ddots & \vdots \\ y_l^T(N-L-1) & y_l^T(N-L) & \cdots & y_l^T(N-1) \end{bmatrix} \tag{10}$$

where N denotes the total number of samples. The pencil parameter L is usually chosen between $N/3$ and $N/2$ in order to achieve filtering noise efficiently. The dimension of the matrix $[Y_l^T]$ is $(N-L) \times (L+1)$. Then, a singular-value decomposition (SVD) is applied to this matrix as $[Y_l^T] = [U][\Sigma][V]^H$, where ^{H} denotes the Hermitian transpose, $[U]$ and $[V]$ are unitary matrices, composed of the eigenvectors of $[Y_l^T][Y_l^T]^H$ and $[Y_l^T]^H[Y_l^T]$, respectively, and $[\Sigma]$ is a diagonal matrix containing the singular values of $[Y_l^T]$. The problem of solving for $\lambda = e^{s_i t}$ can be express as an ordinary eigenvalue problem

$$\{[Y_1]^\dagger[Y_2] - \lambda[I]\} \tag{11}$$

where $[I]$ is an identity matrix and $[Y_1]^\dagger$ is the Moore-Penrose pseudoinverse of $[Y_1]$. The matrix $[Y_1]$ and $[Y_2]$ were defined by deleting the last column and the first column from matrix $[Y_l^T]$, respectively.

C. K-NEAREST NEIGHBOR ALGORITHM

In this paper, the k-NN algorithm is applied in order to create a decision boundary for the extracted poles for the ID detection of the proposed chipless RFID system. The algorithm is one of the classical techniques of non-parametric classifications. The performance of the k-NN algorithm depends upon parameter k, which is the number of found nearest neighbors and distance metric being used to measure the similarity between two samples.

In order to apply the k-NN algorithm to create the decision boundary, the distance which indicates the similarity between a query and label-known training set instances must be calculated first. The training data set $\mathbf{s} = [s_1, s_2, \ldots, s_{N_s}]$ is formed by using poles extracted from the late-time response of all possible tags measured in a free-space anechoic chamber, where N_s denotes the total number of poles being used for training. The individual i^{th} pole $s_i = \sigma_i + j\omega_i$ includes the damping factor σ_i and angular natural frequency ω_i, which are considered as two features of poles. An attribute vector is $a_r(s) = [a_1(s), a_2(s), \ldots, a_\varphi(s)]$ where $a_r(s)$ is the value of the rth attribute of the instance, and φ is the length of the

attribute vector. In this paper, the attribute vector was formed as the pole components of $a_r(s_i) = [\sigma_i, \omega_i]$. The total number of poles being used for training is equal to that of all the poles extracted from all possible tags. The query set $\mathbf{q} = [q_1, q_2, \ldots, q_{Nq}]$ is the set of pixel points obtained from creating a grid of points which uniformly span the entire space within the interval from the minimum complex frequency q_1 to the maximum complex frequency q_{Nq}, where N_q is the total index number of pixel points. The single j^{th} pixel point comprises two features of the complex natural frequency $q_j = \sigma_j' + j\omega_j'$.

There are many distance metrics that one can use in the k-NN method for similarity measurement. The selection of the appropriate distance metric depends upon the context or problem under consideration. Different distance metrics achieve different decision boundaries of detection. First, the most common distance metric is the Euclidean distance, which can be given as

$$d(q_j, s_i) = \sqrt{\sum_{r=1}^{\varphi} \left(a_r(q_j) - a_r(s_i)\right)^2}. \tag{12}$$

Second, the Euclidean distance is generalized and then referred to as the Minkowski distance, whose equation is expressed as

$$d(q_j, s_i) = \left(\sum_{r=1}^{\varphi} \left|a_r(q_j) - a_r(s_i)\right|^p\right)^{1/p}. \tag{13}$$

It is equal to the Euclidean distance when $p = 2$. The third metric is obtained from setting $p = 1$ and is called as the Manhattan distance as given by

$$d(q_j, s_i) = \sum_{r=1}^{\varphi} \left|a_r(q_j) - a_r(s_i)\right|. \tag{14}$$

The Manhattan distance or as it is sometimes called the city block distance, represents the sum of the absolute difference between attribute vectors. The zero of the distance values indicates that the similarity is at a maximum. In contrast, when the distance is high, the similarity between two instances is low.

The fourth metric is the Chebychev distance, which is obtained from a variant of the Minkowski distance. It uses only the most varied attribute variable. The calculation equation of the Chebychev distance is given by

$$d(q_j, s_i) = \max_{r=1}^{\varphi} \left\{\left|a_r(q_j) - a_r(s_i)\right|\right\}. \tag{15}$$

Fifth, the similarity measurement using the Mahalanobis distance is carried out in the space defined by the relevant feature

$$d(q_j, s_i) = \sqrt{\sum_{r=1}^{\varphi} \frac{\left(a_r(q_j) - a_r(s_i)\right)^2}{C_r}} \tag{16}$$

where C_r is a positive definite covariance matrix. Finally, the standardized Euclidean distance, often called the Seuclidean
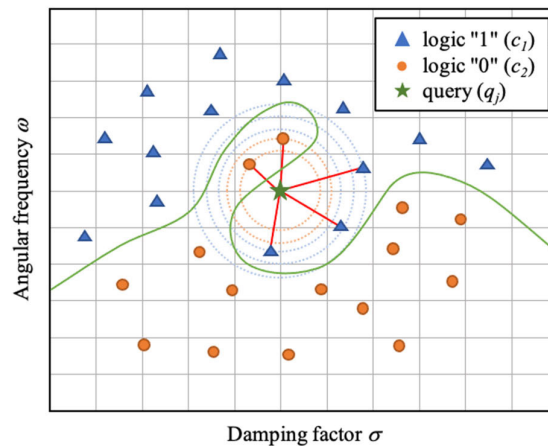

FIGURE 3. An example of decision-boundary creation using the *k*-NN algorithm.

distance, can be calculated by

$$d(q_j, s_i) = \sqrt{\sum_{r=1}^{\varphi} \frac{\left(a_r(q_j) - a_r(s_i)\right)^2}{V_r}} \tag{17}$$

where V_r is the standard deviation.

In order to create the decision boundary for ID detection, the class label can take two values as logic "1" or logic "0," denoted by $\mathbf{c} = [c_1, c_2]$. All of the poles in the training set are labeled and the distance is measured from every pixel point. The set $\mathbf{u} = [u_1, u_2, \ldots, u_k]$ with k minimum distances is chosen from the training data set $\mathbf{s}$, where k is the number of nearest neighbors. The k-NN algorithm assigns the query to the most frequently occurring class of its k neighbors using the majority voting rule by the Kronecker delta. The class label of the query can be expressed as

$$c(q_j) = \arg\max_{c \in \mathbf{c}} \sum_{i=1}^{k} \delta(c, c(u_i)) \tag{18}$$

where

$$\delta(c, c(u_i)) = \begin{cases} 0, & c \neq c(u_i) \\ 1, & c = c(u_i). \end{cases} \tag{19}$$

Fig. 3 illustrates an example of decision-boundary creation using the k-NN algorithm. There are two features, the damping factor σ and angular natural frequency ω, being used to identify the logic of each pixel point in the whole boundary. In the figure, the training data, referred to as poles pre-labeled as logic "1" and logic "0," are denoted by a triangle and circle, respectively, while an unknown class query referred to as a pixel point is denoted by a star. For this example, the Euclidean distance was applied to calculate the similarity measurement. The red lines represent the Euclidean distance between poles s_i and pixel point q_j. According to Fig. 3, if k is chosen to be 2, the two nearest neighbors are poles labeled by the logic "0." Thus, the pixel point which is denoted by a star will be classified as logic "0" as well. On the other hand, if k
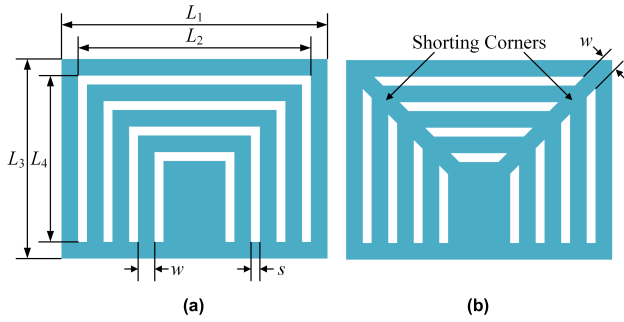
FIGURE 4. Structural layout of the chipless RFID tags with its IDs of (a) "1111" (b) "0000."
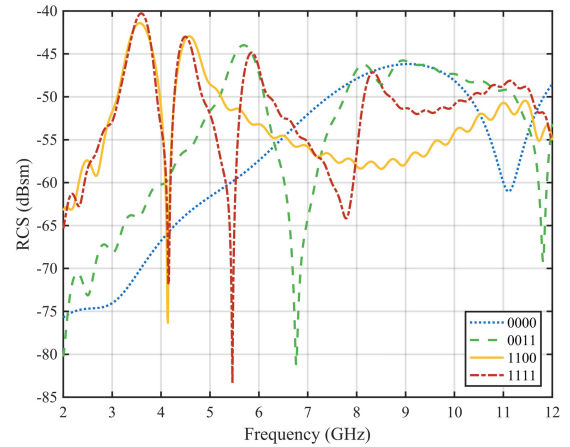

FIGURE 5. Simulated RCS spectra of the chipless RFID tags.

is chosen to be 5, two and three nearest neighbors are poles labeled by logic "0" and "1," respectively. Thus, this pixel will be classified as logic "1" because of the greatest number of nearest neighbors labeled as logic "1." Note that the value of k affects the sensitivity of the k-NN classifier. Finding an appropriate value of k is required. Besides choosing the appropriate value of k, misclassification should be minimized by selecting the distance metrics. As mentioned, in this paper, the decision boundary created by using the k-NN algorithm is exploited in order to detect the ID of tags attached to the containers that affect pole changes. The area region corresponding to the number of pixels defined as logic "1" should be the largest. The number of pixels defined by logic "1" is given by

$$N_p = \sum_{j=1}^{Nq} \left(c(q_j) = c_1 \right). \tag{20}$$

III. DECISION-BOUNDARY CREATION
A. TAG DESIGN
The chipless RFID tag employed to demonstrate the proposed technique was a rectangular metallic patch loaded with four slot resonators [26]. Fig. 4(a) and (b) depict examples of the structural layout of the chipless RFID tag with IDs of "1111" and "0000," respectively. The tag consisting of a rectangular patch and slot resonators was designed and then fabricated on the single layer FR4, whose dielectric constant and loss tangent were 4.4 and 0.014, respectively. The thickness of the substate and copper was 0.8 mm and 0.035 mm, respectively. The adjustable resonant frequency of the tag depends upon the length and width of the slots. Four different-size slot resonators were placed on the FR4 in order to attain four different resonant frequencies. The longest and shortest slots represent the most significant bit (MSB) and least significant bit (LSB) indicated by the lowest and highest resonant frequencies, respectively. According to the Fig. 4, the parameters are of sizes $L_1 = 12$ mm, $L_2 = 10.5$ mm, $L_3 = 9$ mm, $L_4 = 7.5$ mm, $w = 0.75$ mm and $s = 0.4$ mm. The sixteen possible bit IDs can be achieved by easily shorting and/or opening the slots at the corners of the rectangular patch.

The simulations of the tags were conducted by using CST Microwave Studio in order to validate the desirable resonant frequency. In simulations, the tag was placed in the free space with the boundary setting of "open add space" for all axis directions. The tag was excited by a plane wave directed along the positive z-axis in order to generate its RCS spectrum, as seen in Fig. 5. In the figure, peaks corresponding to the resonant frequencies of the tag ID of "1111" appear at 3.59, 4.48, 5.81, and 8.32 GHz. After shorting and opening the slots at the corners of the rectangular patch, the peak corresponding to the resonant frequency of the shorted-slot line disappears while that of the opened-slot line still exists or does not significantly change.

B. EXPERIMENTAL SETUP
This section discusses the experiments conducted in order to create the decision boundary for the detection of the chipless RFID system. The experiments were done in an anechoic chamber under a bistatic set-up configuration, as seen in the Fig. 6. The transmitting and receiving antennas were the ultra-wideband tapered slot antennas proposed in [27]. The measured return loss of the antennas was below –10 dB from 3.1 to 10.6 GHz, which covers all of the resonant frequencies of the chipless RFID tags. The average gain of the antennas at the frequency of 6.5-8.5 GHz was 10.5 dBi. The antennas were placed in a face-to-face orientation and 6 cm away from each other. The fabricated chipless RFID tag was placed on the sample holder made of Styrofoam whose dielectric constant was approximately unity. Although the tag was placed in other directions, its poles do not change because they are aspect independent [11]. The distance between the tag and the center of the antennas was 10 cm. The R&S ZVB20 vector network analyzer (VNA) was used to measure scattering coefficient S_{21} and the delivered power was set as 0 dB. The swept frequency interval was 10 MHz and the total sample of each measurement was 1001. All of the measurements in the frequency range between 2 and 12 GHz were repeated 10 times and averaged for accuracy and reliability.
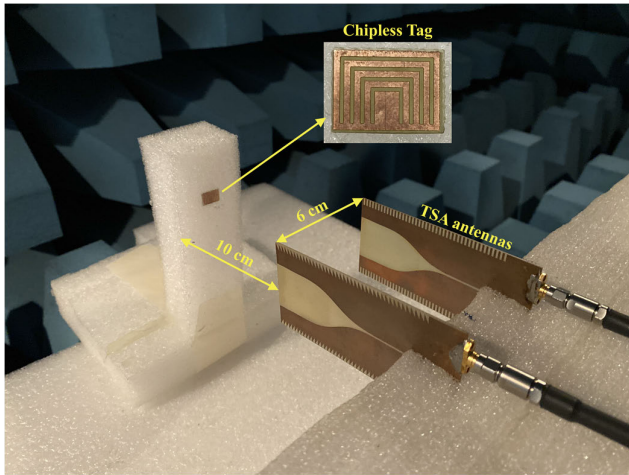
FIGURE 6. Experimental setup of the chipless RFID system in the anechoic chamber.

The distance between the tag and antennas does not affect extracted poles [17]. However, the distance or called read range should be maximized [28], [29]. Here, the effect of the distance between the tag and antennas was not taken into account because it depends upon several parameters, such as delivered power, antenna gain, VNA sensitivity, etc.

As mentioned, antenna calibration is required in order to reduce the antenna effect, including antenna mutual coupling and antenna response variation. In the antenna calibration, the large metal plate of 50 cm × 50 cm was placed instead of the tag in order to be a reference $H_{plate}(\omega)$. It was assumed that the plate perfectly reflected all of the incident electromagnetic (EM) waves. Further, scattering coefficient S_{21} was also measured without any tag in order to obtain $H_{no\ tag}(\omega)$. $H_{plate}(\omega)$ and $H_{no\ tag}(\omega)$ were used to perform the antenna calibration according to (5).

C. POLE EXTRACTIONS

In this paper, the STMPM was applied to the proposed chipless RFID detection system in order to extract poles from the tag response obtained from the measurement for the scattering coefficient S_{21}, as discussed above. Before extracting the poles, the tag response in the frequency domain was transformed to that in the time domain by using the inverse Fourier transform. Fig. 7(a) and (b) depict the trajectories of the four pair poles obtained from the STMPM with and without the antenna calibration, respectively. The poles, including natural frequencies and the damping factor as plotted in Fig. 7(a) and (b), show their clumps. According to Fig. 7(a), for example, the average natural frequencies of tag ID of "0000" at the late time $t_L = 0.832$ *n*s were 2.0553, 3.0593, 3.8350, and 12.0150 GHz, while those of tag ID of "1111" were 2.9320, 3.7218, 6.4468, and 12.015 GHz, respectively. There are some almost identical natural frequencies being used to detect logic "0" or logic "1."
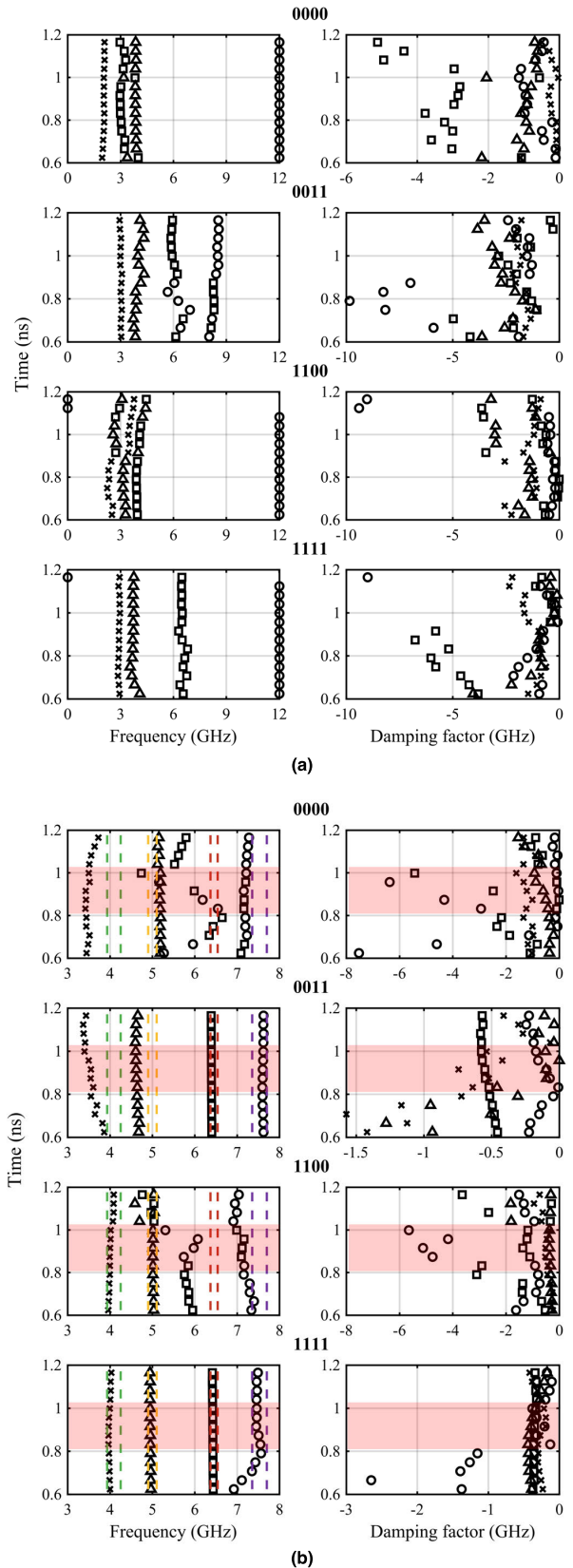
FIGURE 7. Poles extracted by using the STMPM (a) without calibration (b) with calibration.

TABLE 1. Average poles extracted from the late-time response by using STMPM (GHz).

tag IDs	1st bit σ	1st bit f	2nd bit σ	2nd bit f	3rd bit σ	3rd bit f	4th bit σ	4th bit f
0000	-1.3079	3.4767	-0.7205	5.1683	-1.7600	6.1226	-2.1859	6.5857
0001	-0.0846	3.5295	-0.1204	4.6329	-0.4512	6.1151	-0.2629	7.5729
0010	-0.6725	3.6267	-0.8512	4.7208	-0.6872	5.4172	-0.5950	6.4371
0011	-0.4581	3.4789	-0.0106	4.6103	-0.5631	6.3912	-0.1367	7.6115
0100	-1.0899	3.4515	-0.4284	4.6395	-0.2840	5.0695	-0.1751	7.0469
0101	-0.1526	3.4866	-0.3380	4.9985	-0.1646	6.1113	-0.1298	7.4954
0110	-0.1363	3.6722	-0.3583	4.9681	-0.6196	6.4611	-0.8759	6.8850
0111	-0.2339	3.6781	-0.4510	4.9374	-0.5431	6.4085	-0.1669	7.4869
1000	-0.3388	4.0553	-0.9496	5.1601	-0.1491	6.1274	-0.5427	7.1949
1001	-0.3273	4.0875	-0.1172	4.6254	-0.0955	6.7802	-0.0044	7.5574
1010	-0.2824	4.0029	-1.5803	4.6275	-0.1507	5.9275	-0.4418	6.4790
1011	-0.2130	4.0146	-1.0777	5.2019	-0.5663	6.4100	-0.2474	7.3992
1100	-0.5093	4.0170	-0.6602	4.9490	-1.0421	6.6810	-4.1300	6.0009
1101	-0.3427	4.0297	-0.2985	5.0382	-0.2296	6.0874	-0.1170	7.4347
1110	-0.2260	3.9961	-0.4014	4.9803	-0.0353	5.8168	-0.4812	6.4916
1111	-0.2253	3.9811	-0.3639	4.9463	-0.3374	6.4228	-0.1576	7.4675

FIGURE 8. Decision boundary of the LSB of the proposed chipless RFID.

Thus, detection of the natural frequencies as logic "0" or "1" is not clearly visible when antenna calibration is not used. Obtained from performing the antenna calibration, the STMPM-based extracted poles plotted in Fig. 7(b) can detect the logic "0" or logic "1." The frequency range of detecting logic "1" for the first order (MSB) to the fourth order (LSB) was 3.932-4.25 GHz, 4.9-5.1, 6.37-6.54, and 7.355-7.7 GHz, respectively. These frequency ranges were obtained using half of the Euclidean distance calculated from the nearest poles of logic "0" and logic "1" of each order.

As an example of the tag ID of "0011," the average natural frequencies at the late time highlighted in pink were 3.4789, 4.6103, 6.3912, and 7.6115 GHz, respectively. The third and fourth orders of 6.3912 and 7.6115 GHz were in the frequency ranges of 6.37-6.54 and 7.355-7.7 GHz, respectively. This reveals that the third and fourth orders of these extracted natural frequencies can represent logic "1." In contrast, the first and second orders of 3.4789 and 4.6103 GHz were out of the frequency ranges of 3.932-4.25 and 4.9-5.1 GHz, respectively.

This indicates that these extracted natural frequencies represent logic "0." It should be noted that in order to detect the tag IDs by using only the natural frequency, the frequency range for detection was somewhat narrow. Table 1 summarizes the average poles extracted from the late-time response by using the STMPM. With only extracted natural frequencies, they were detected as logic "1," which was highlighted in red, as seen in the table. Moreover, it is important to note that the frequency range in which the extracted frequency order was detected as to whether it was logic "1" or "0" was very narrow. This implies that the chipless RFID detection system using only the extracted natural frequency was sensitive to the application environments resulting in the pole perturbation.

D. DECISION BOUNDARY
The scattering coefficients S_{21} of all of the individual sixteen tags with their possible IDs from "0000" to "1111"
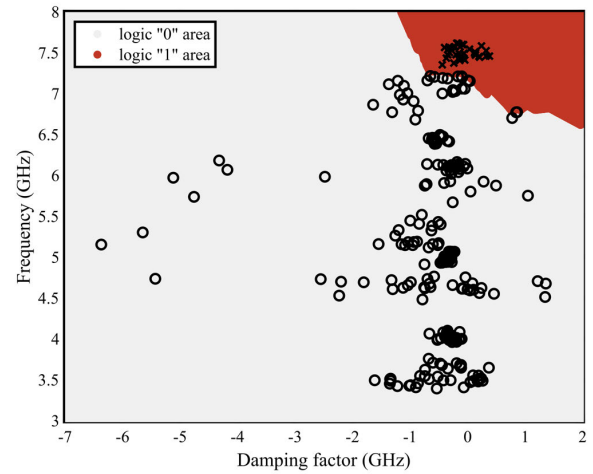
were measured in order to create the decision boundary for ID detection. An antenna calibration was also performed in order to achieve $H_{tag}(\omega)$ for all of the tags. Then, taking the inverse Fourier transform to transfer function $H_{tag}(\omega)$ with respect to variable t gives tag response $h_{tag}(t)$ in the time domain. The STMPM was applied to extract the poles being used to represent the tag IDs. The number of order of poles extracted by using the STMPM was four, corresponding to the bits of a tag. For each order, five successive poles, including the natural frequencies and damping factors, were chosen from the late-time portion starting at $t_L = 0.832$ ns for the ID detection of the individual bit. Thus, the total number of chosen poles exploited to create the decision boundary of the proposed chipless RFID system with sixteen possible chipless RFID tags was equal to $16 \times 4 \times 5 = 320$. The numbers 16, 4, and 5 indicate the number of tags, the order of extracted poles, and the number of the successive chosen poles of each order, respectively. These chosen poles were exploited as training instances. In order to create the decision boundary, the individual bit of a tag was determined. For example, the total of 320 poles was divided into two data classes for creating the decision boundary of the LSB. The first data class contained 40 poles, which were labeled as logic "1" of eight possible IDs of the LSB. In the second class, the 280 other poles left were labeled as logic "0." The minimum and maximum of the pole values, including natural frequencies and damping factors, were used to find the whole boundary of pixels of the decision.

The 2D grid for the whole decision boundary was created with a uniform area whose one pixel was represented by 5 MHz × 5 MHz. The similarity based on five different distance metrics, i.e. Euclidean, city block, Chebychev, Mahalanobis, and Seuclidean distances was measured. Based on the k-NN algorithm, the number of nearest neighbors was first chosen as $k = 1$ in order to measure the similarity and then increased so that the maximum pixel number N_p of the region defined as logic "1" was achieved with the condition

TABLE 2. Maximum pixel number of logic "1" (N_P) and neighbors (k).

distance	1st bit		2nd bit		3rd bit		4th bit	
metrics	N_p	k	N_p	k	N_p	k	N_P	k
Euclidean	6842	20	4310	8	6504	9	29625	16
city block	11531	20	4059	8	6274	10	24032	18
Chebychev	6457	20	3960	6	4317	4	16177	6
Mahalanobis	5136	15	3661	6	4036	6	23564	10
Seuclidean	5179	16	3630	6	3986	6	26340	12
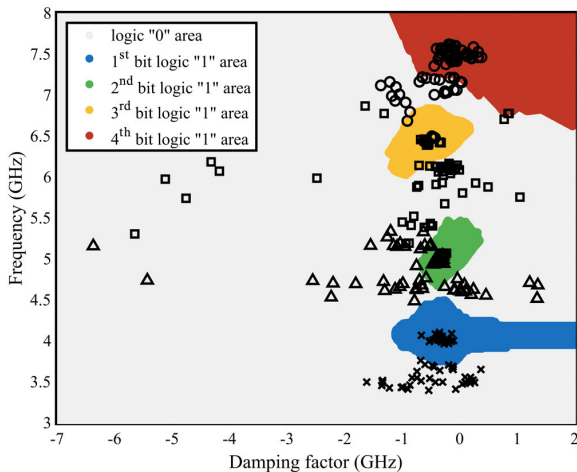
FIGURE 9. Whole decision boundary of the proposed chipless RFID.

that there was no error for the classification between the two training data classes. With the Euclidean distance method, the maximum pixel number $N_p = 29{,}625$ was achieved when $k = 16$. These parameters were used to create the decision boundary of the LSB. The decision boundary of the LSB, created by using the k-NN algorithm, is depicted in Fig. 8. The red and grey areas are defined as logic "1" and "0," respectively. In order to detect the tag ID, if the extracted poles which represent the LSB are in the red area, they will be detected as logic "1" and *vice versa*.

In order to create the decision boundary of the other bits remaining, dividing the poles into two classes was performed again. The first class, which was labeled as logic "1," contains the extracted poles representing logic "1" of the determined bit. The other poles that remain, representing the other bits and logic "0" of the determined bit, were labeled as logic "0" in the second class. The k nearest neighbors was investigated using five different distance metrics, i.e. Euclidean, city block, Chebychev, Mahalanobis, and Seuclidean distances, in order to maximize the pixel number N_p of the boundary defined as logic "1" as well. The maximum pixel number N_p is required because in practical terms, the chipless RFID tag will be attached to the container, resulting in perturbation of the extracted pole defined as logic "1" of the bit of tags. The larger decision boundary keeps the perturbed pole in the correct classification.

Table 2 summarizes the k nearest neighbors and boundary pixel number N_p of the individual bit of the chipless RFID

tags using the distance-based similarity measurement with five different distance metrics. In the table, the chosen k that achieves the maximum pixel number N_p of the decision boundary of logic "1" of the individual tag bit is highlighted in red. The decision boundary of the individual bit of tags was created by using the k-NN algorithm along with the red-highlighted parameters shown in the table, and then these were combined. Fig. 9 depicts the entire decision boundary of all of the bits of the proposed chipless RFID system. The blue, green, yellow, and red regions stand for the boundary of logic "1" of the first (MSB), second, third, and fourth (LSB) bits, respectively. The extracted poles that have fallen into these regions will be detected as logic "1" for the determined bit. It should be noticed that this decision boundary is only for these specific chipless RFID tags. If another tag type is used, re-creating the decision boundary is then required.

IV. DETECTION OF THE CHIPLESS RFID SYSTEM

The chipless RFID tag should be particularly designed for placing it on the container with the given material characteristic. However, this is expensive and difficult to redesign for a new item of the container. Instead of redesigning the tag, the calibration is also introduced in order to reduce the unwanted effect due to the container's characteristic and other surrounding environments. The main purpose of the use of the calibration is to mitigate the effect due to the frequency response variation and mutual coupling caused by the antenna [11], [16], [17]. In fact, calibration cannot completely remove the unwanted effect. In spite of using calibration, the poles exploited here to represent the tag ID could change when the tag is attached to the container.

In this section, the effect of the container on the detection performance of the proposed chipless RFID system was investigated *via* experiments. These experiments were set up in order to take the effect of the container on the detection performance of the proposed chipless RFID system into account. In our experiments, the chipless RFID tag was attached to the container, as depicted in Fig. 10. The experiments were divided into four different cases with different containers and different positions of tags attached to the containers. In the first and second cases, a tag was attached respectively outside and inside the lid of the container, which was a parcel box made of paper. For the third and fourth cases, a tag was attached outside and inside the lid of a plastic box, respectively. The dimensions of the parcel and plastic boxes were 30 cm × 20 cm × 11 cm and 32 cm × 22 cm × 11 cm, respectively.

The experimental setup was conducted in an anechoic chamber in order to avoid the effect of the surrounding environments. The configuration of the setup was the same as that of the experiment for creating the decision boundary, described in the previous section. The calibration was performed in order to remove the unwanted effects due to the antenna and environments. In the calibration process, the scattering coefficients S_{21} of the tag attached to the container were measured in order to obtain $H_{total}(\omega)$. A large

TABLE 3. Average extracted natural frequencies (GHz) for conventional ID detection.

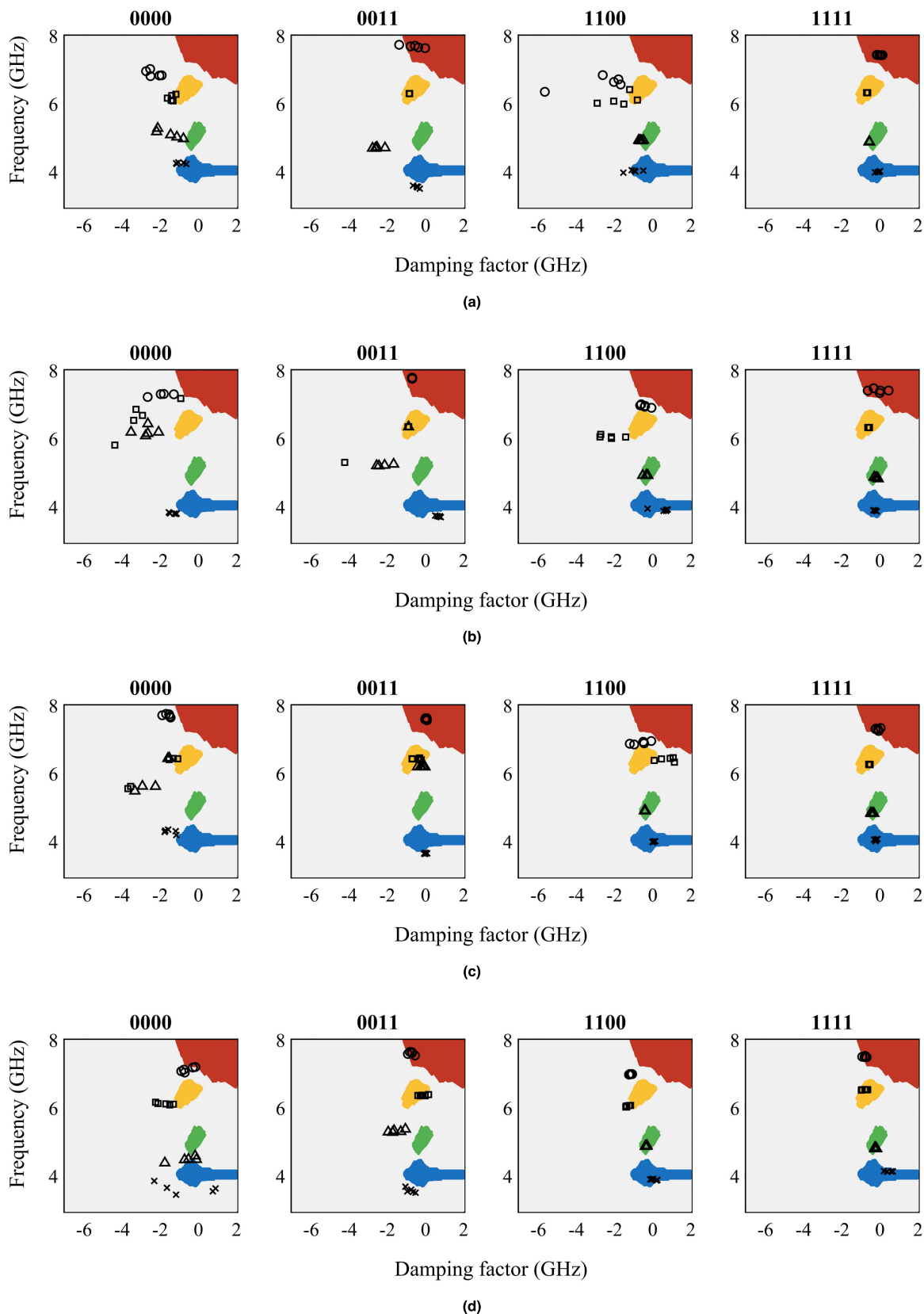| tag IDs	parcel box								plastic box							
	outside				inside				outside				inside			
	1st bit	2nd bit	3rd bit	4th bit	1st bit	2nd bit	3rd bit	4th bit	1st bit	2nd bit	3rd bit	4th bit	1st bit	2nd bit	3rd bit	4th bit
0000	4.276	5.132	6.199	6.916	3.831	6.232	6.634	7.227	4.313	5.948	6.115	7.728	3.651	4.508	6.146	7.150
0001	3.611	5.167	6.769	7.074	4.445	5.972	6.963	7.742	3.666	5.747	6.798	7.687	3.628	6.008	7.213	6.929
0010	4.020	4.888	5.753	6.547	3.743	6.348	6.870	6.848	4.358	5.491	6.087	7.623	3.656	5.483	6.222	6.942
0011	3.579	4.726	6.323	7.708	3.744	5.467	6.159	7.798	3.675	6.218	6.452	7.621	3.597	5.340	6.393	7.629
0100	3.715	4.935	6.124	7.056	3.739	4.935	6.161	7.488	4.450	4.957	6.308	7.627	3.880	4.885	6.356	7.199
0101	3.666	4.950	6.555	7.465	3.722	4.936	6.374	7.362	4.933	5.174	6.276	7.582	4.460	4.904	6.795	7.565
0110	3.800	4.858	6.309	7.203	3.709	4.909	6.381	6.818	4.454	4.901	6.320	6.961	3.786	4.828	6.281	7.724
0111	3.660	4.872	6.328	7.429	3.691	4.865	6.308	7.268	4.801	4.966	6.274	7.512	3.492	4.812	6.399	7.514
1000	3.974	5.926	6.934	6.634	3.995	4.567	6.754	7.546	3.981	5.183	6.409	7.852	4.000	5.689	6.760	6.658
1001	4.002	5.395	6.110	7.590	3.688	4.044	7.001	7.772	3.988	5.616	6.806	7.592	3.947	5.889	6.897	7.436
1010	3.971	4.667	6.390	5.853	3.985	4.479	6.411	7.268	3.995	5.395	6.388	6.589	3.992	5.975	6.198	7.140
1011	3.993	5.170	6.335	7.477	3.919	6.288	6.673	7.643	3.985	6.024	6.198	7.584	3.971	5.692	6.272	7.451
1100	4.044	4.944	6.147	6.648	3.931	4.945	6.079	6.978	4.020	4.928	6.433	6.923	3.917	4.899	6.075	7.012
1101	4.018	4.953	6.806	7.498	3.846	4.981	6.853	7.788	4.025	4.943	6.752	7.441	3.971	4.903	5.955	7.515
1110	4.055	4.915	6.440	7.246	3.910	4.892	6.404	7.097	4.016	4.895	6.407	6.918	3.970	4.851	6.324	7.098
1111	4.025	4.906	6.349	7.457	3.909	4.872	6.347	7.430	4.069	4.852	6.288	7.326	4.158	4.835	6.557	7.527

(a)
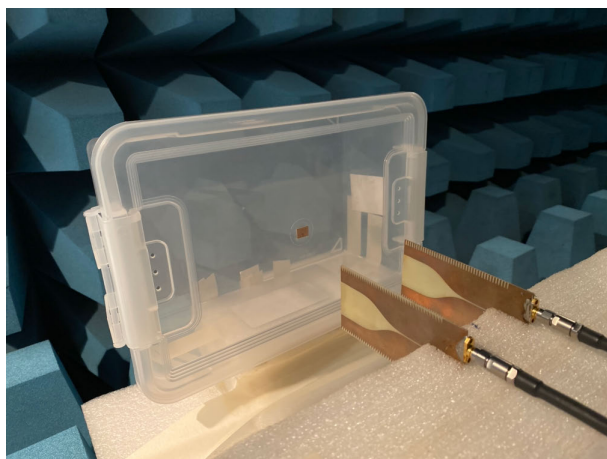
(b)

FIGURE 10. Experimental setups of the chipless RFID system with tags (a) outside the parcel box (b) inside the plastic box.

metal plate was placed instead of the container and tag in order to perfectly reflect all of the incident EM waves. The $H_{plate}(\omega)$ was therefore obtained from the measurement.

In order to obtain $H_{no\ tag}(\omega)$, the measurement without any tag was performed. The $H_{total}(\omega)$, $H_{plate}(\omega)$, and $H_{no\ tag}(\omega)$ were substituted into (5) in order to attain $H_{tag}(\omega)$. The inverse Fourier transform was used to transform $H_{tag}(\omega)$ to time-domain response $h_{tag}(t)$. The tag response $h_{tag}(t)$ in the time domain was exploited in order to extract the poles, including the natural frequencies and damping factors. The five successive poles in the late time were chosen for the chipless RFID detection. The experiments were repeated for all sixteen possible tags.

The five successive natural frequencies of any bit of a tag were averaged, and the average frequency was exploited in order to detect the tag ID. Table 3 summarizes the averaged value of the extracted natural frequency. The detection range can be calculated by a half of the Euclidean distance between the nearest natural frequencies defined as logic "0" and logic "1" of each order, as mentioned in the previous section. The detection range of the first, section, third, and fourth bits of logic "1" of all sixteen tags was 3.932-4.25 GHz, 4.9-5.1 GHz, 6.37-6.54 GHz, and 7.355-7.7 GHz, respectively. If the averaged value of the extracted natural frequencies in the late time fell in these frequency ranges, the underlying frequency was detected as logic "1," and *vice versa*. The experimental results of the natural frequency extracted from the response of the tag attached inside and outside the parcel and plastic boxes are summarized in the Table 3. Some of the extracted natural frequencies which should be detected as logic "1" are out of the detection frequency range, as highlighted in red. Thus, the detection for logic "1" of these frequencies out of the detection frequency range was not correct. On the other hand, the extracted natural frequencies represented as logic "0" should be out of the detection frequency range but they fell in the range. This detection became not correct as well.

The percentage of the fault detection of the tag attached outside and inside the parcel box and outside and inside the plastic box was 15.625%, 32.8125%, 26.5625%,

FIGURE 11. Tag ID detection of the proposed chipless RFID system with tags attached (a) outside the parcel box (b) inside the parcel box (c) outside the plastic box, and (d) inside the plastic box.

TABLE 4. Percentage of ID detection.

criteria	natural frequency only				proposed method			
	parcel box		plastic box		parcel box		plastic box	
	outside	inside	outside	inside	outside	inside	outside	inside
three-fifths	62.5%	31.25%	37.5%	37.5%	100%	100%	100%	100%
all poles	83.13%	67.5%	75.94%	76.88%	95.63%	95.94%	95.31%	95%
1st bit	100%	72.5%	95%	92.5%	97.5%	97.5%	97.5%	96.25%
2nd bit	82.5%	77.5%	80%	62.5%	92.5%	93.75%	96.25%	100%
3rd bit	57.5%	66.25%	50%	58.75%	95%	93.75%	90%	91.25%
4th bit	92.5%	53.75%	78.75%	93.75%	97.5%	98.75%	97.5%	92.5%

and 25%, respectively. It can be seen that, using the extracted natural frequency only, the effect of the container degrades the performance of the chipless RFID detection. The fault detection rate of the tag attached inside the lid of the parcel box was highest. This implies that the parcel box affects the detection performance the most. The percentage of the fault detection of the first, second, third, and fourth bits of the tag attached to all of the container cases was 12.5%, 25%, 37.5%, and 25%, respectively. Thus, the third bit of tags was the most sensitive to the container. However, the detection rate needed in a practical situation could be 100 percent. The fault detection implies that the use of only the natural frequency of chipless RFID detection is not suitable for packaging applications.

The use of poles, including the natural frequency and damping factor, was therefore introduced in order to detect the bit logic of the chipless RFID tag. For the detection, the decision boundary must first be created, as discussed in the previous section. The created decision boundary depicted in Fig. 9 shows the regions for detection of the logic of four bits of chipless RFID tags. In order to investigate the performance of the proposed chipless RFID detection system using poles along with the k-NN algorithm, experiments for all sixteen possible tags attached to the container were conducted. After performing the calibration and frequency-to-time domain transform, the STMPM was exploited in order to extract poles from the tag's response $h_{tag}(t)$ in the time domain. For each pole order corresponding to the bit order of a tag, five successive poles at the late time were chosen for the chipless RFID detection system; and in order to detect the bit logics of a tag, all twenty poles of all four orders obtained from the response of a tag were fed into the decision boundary. If the poles fell into the colored region of the decision boundary, as seen in Fig. 9, these poles were detected as logic "1." On the other hand, poles were detected as logic "0" if they were outside the colored region. This detection process was repeated for other bits of a tag.

Fig. 11 depicts some examples of the experimental ID detections of the proposed chipless RFID system in cases of tags attached outside and inside the parcel boxes and outside and inside the plastic boxes. In the figure, the tag IDs of "0000," "0011," "1100," and "1111" were examined. For each tag, twenty poles extracted by using STMPM fell into the decision boundary created by using the k-NN algorithm in

order to detect its ID. The cross, triangle, rectangle, and circle symbols denote the poles of the first (MSB), second, third, and fourth (LSB) bits, respectively. As seen in the figure, the poles obtained from the tags attached at different positions of different containers changed from those obtained from the tags measured in the free space. Fig. 11(a) depicts the ID detection of the proposed chipless RFID system with tags attached outside the parcel box. For example, of the tag ID of "0011," all five poles of the first and second orders that slipped out of the blue and green regions were detected as logic "0." Since all five poles of the third bit fell into the yellow region, this bit was detected as logic "1." However, for the LSB, a pole slipped out of the red region. The decision criteria for logic "1" or "0" should be determined. In this paper, we determine the decision criteria with more than three-fifths of the five successive poles extracted from the response of a tag under consideration in order to detect the bit logic of "1" or "0." Since the number of poles in the red region is greater than that of poles that slipped out of the red region, the LSB was detected as logic "1." Likewise, the detection of the ID "0000" of a tag attached inside the plastic box is shown in Fig. 11(d). We applied the decision criteria with more than three-fifths of the five successive extracted poles. The tag ID was detected as "0000" correctly.

Table 4 summarizes the performance of the decision criteria of the proposed chipless RFID system using poles along with the k-NN algorithm and the conventional chipless RFID system using only the natural frequency. According to the table, the use of the decision criteria with more than three-fifths of the five successive extracted poles to detect logic "1" or "0" achieves 100% of the proposed detection, although there exist pole changes due to the container. Unfortunately, using the decision criteria with more than three-fifths of the five successive extracted poles, the detection rates of the use of only the natural frequency were 62.5%, 31.25%, 37.5%, and 37.5% for the tags attached outside and inside the parcel boxes and outside and inside the plastic boxes, respectively. These detection rates are very low, implying that the use of only the natural frequency is not suitable for the ID detection of the chipless RFID system used in the practical situations of attachment of tags to the container.

Using another decision criterion, the individual bit of tags was determined. For example, the first, second, third, and fourth bits of tags attain different detection rates of different

tools, i.e. pole and only natural frequency for detection. The detection rates were not 100%. This reveals that there are changes of some poles and natural frequencies of tags attached to the container. However, the proposed chipless RFID system using the poles along with the k-NN algorithm still achieves a 100% detection rate for suitable decision criteria. Thus, the proposed chipless RFID detection system is robust from the effect of the container.

V. CONCLUSION

In this paper, a detection technique of the chipless RFID system has been proposed. The technique applies the STMPM to extract poles from the tag's response. The poles of all possible tags measured in the free-space anechoic chamber were exploited in order to create a decision boundary by using the k-NN algorithm. Experiments with the chipless RFID system with tags attached to the containers were conducted in order to investigate the pole changes that impact detection performance. The experimental results obtained from detection using the proposed and conventional techniques were compared, and the detection rates using the conventional detection technique using only natural frequency were 62.5%, 31.25%, 37.5%, and 37.5% for cases of tags attached outside and inside the parcel boxes and outside and inside the plastic boxes, respectively. With the proposed technique, the detection rate calculated from all poles has been improved at 95.63%, 95.94%, 95.31%, 95% for cases of tags attached outside and inside the parcel boxes and outside and inside the plastic boxes, respectively. The detection rate of the proposed technique along with the decision criteria with more than three-fifths of five successive extracted poles have achieved 100% for all cases. The experimental results have demonstrated the superiority of the proposed technique over the conventional one. However, one of the limitations of the proposed technique is the operation scenario with one reader and one tag. A technique for detecting multiple chipless RFID tags will be presented in a future publication.

REFERENCES

[1] V. P. Plessky and L. M. Reindl, "Review on SAW RFID tags," *IEEE Trans. Ultrason., Ferroelectr., Freq. Control*, vol. 57, no. 3, pp. 654–668, Mar. 2010, doi: 10.1109/TUFFC.2010.1462.

[2] A. Stelzer, S. Scheiblhofer, S. Schuster, and R. Teichmann, "Wireless sensor marking and temperature measurement with SAW-identification tags," *Measurement*, vol. 41, no. 5, pp. 579–588, Jun. 2008, doi: 10.1016/j.measurement.2007.02.004.

[3] J. Vemagiri, A. Chamarti, M. Agarwal, and K. Varahramyan, "Transmission line delay-based radio frequency identification (RFID) tag," *Microw. Opt. Technol. Lett.*, vol. 49, no. 8, pp. 1900–1904, Aug. 2007, doi: 10.1504/IJRFITA.2007.017749.

[4] S. Shretha, J. Vemagiri, M. Agarwal, and K. Varahramyan, "Transmission line reflection and delay-based ID generation scheme for RFID and other applications," *Int. J. Radio Freq. Identificat. Technol. Appl.*, vol. 1, no. 4, pp. 401–416, 2007, doi: 10.1504/IJRFITA.2007.017749.

[5] Y. Wang, C.-H. Quan, F.-X. Liu, X.-Y. Zhang, and J.-C. Lee, "A new chipless RFID permittivity sensor system," *IEEE Access*, vol. 9, pp. 35027–35033, 2021, doi: 10.1109/ACCESS.2021.3060467.

[6] K. Suresh, V. Jeoti, S. Soeung, M. Drieberg, M. Goh, and M. Z. Aslam, "A comparative survey on silicon based and surface acoustic wave (SAW)-based RFID tags: Potentials, challenges, and future directions," *IEEE Access*, vol. 8, pp. 91624–91647, 2020, doi: 10.1109/ACCESS.2020.2976533.

[7] S. Dey, J. K. Saha, and N. C. Karmakar, "Smart sensing: Chipless RFID solutions for the internet of everything," *IEEE Microw. Mag.*, vol. 16, no. 10, pp. 26–39, Nov. 2015, doi: 10.1109/MMM.2015.2465711.

[8] S. Preradovic, S. M. Roy, and N. C. Karmakar, "RFID system based on fully printable chipless tag for paper-/plastic-ltem tagging," *IEEE Antennas Propag. Mag.*, vol. 53, no. 5, pp. 15–32, Oct. 2011, doi: 10.1109/MAP.2011.6138421.

[9] W. M. Abdulkawi and A.-F.-A. Sheta, "K-state resonators for high-coding-capacity chipless RFID applications," *IEEE Access*, vol. 7, pp. 185868–185878, 2019, doi: 10.1109/ACCESS.2019.2961565.

[10] M. E. B. Jalil, M. K. A. Rahim, H. Mohamed, N. A. B. Samsuri, N. A. Murad, R. Dewan, H. B. A. Majid, N. B. M. Nafis, L. O. Nur, and B. S. Nugroho, "High capacity and miniaturized flexible chipless RFID tag using modified complementary split ring resonator," *IEEE Access*, vol. 9, pp. 33929–33943, 2021, doi: 10.1109/ACCESS.2021.3061792.

[11] A. T. Blischak and M. Manteghi, "Embedded singularity chipless RFID tags," *IEEE Trans. Antennas Propag.*, vol. 59, no. 11, pp. 3961–3968, Nov. 2011, doi: 10.1109/TAP.2011.2164191.

[12] A. Boonpoonga, P. Chomdee, S. Burintramart, and P. Akkaraekthalin, "Simple estimation of late-time response for radar target identification," *Radio Sci.*, vol. 52, no. 6, pp. 456–743, 2017, doi: 10.1002/2016RS006237.

[13] N. Chantasen, A. Boonpoonga, S. Burintramart, K. Athikulwongse, and P. Akkaraekthalin, "Automatic detection and classification of buried objects using ground-penetrating radar for counter-improvised explosive devices," *Radio Sci.*, vol. 53, no. 2, pp. 210–227, Feb. 2018, doi: 10.1002/2017RS006402.

[14] R. Rezaiesarlak and M. Manteghi, "Short-time matrix pencil method for chipless RFID detection applications," *IEEE Trans. Antennas Propag.*, vol. 61, no. 5, pp. 2801–2806, May 2013, doi: 10.1109/TAP.2013.2238497.

[15] N. Chantasen, A. Boonpoonga, K. Athikulwongse, K. Kaemarungsi, and P. Akkaraekthalin, "Mapping the physical and dielectric properties of layered soil using short-time matrix pencil method-based ground-penetrating radar," *IEEE Access*, vol. 8, pp. 105610–105621, Feb. 2020, doi: 10.1109/ACCESS.2020.2999894.

[16] L. Bannawat, A. Boonpoonga, S. Burintramart, and P. Akkaraekthalin, "On the resolution improvement of radar target identification with filtering antenna effects," *Int. J. Antennas Propag.*, vol. 2018, pp. 1–11, 2018, doi: 10.1155/2018/3405908.

[17] L. Bannawat, A. Boonpoonga, and P. Akkaraekthalin, "Permittivity estimation of a shallow-layered medium using high-resolution ground-penetrating radar," *Int. J. Remote Sens.*, vol. 41, no. 12, pp. 4624–4641, Jun. 2020, doi: 10.1080/01431161.2020.1723177.

[18] R. Rezaiesarlak and M. Manteghi, "Complex-natural-resonance-based design of chipless RFID tag for high-density data," *IEEE Trans. Antennas Propag.*, vol. 62, no. 2, pp. 898–904, Feb. 2014, doi: 10.1109/TAP.2013.2290998.

[19] A. Vena, E. Perret, D. Kaddour, and T. Baron, "Toward a reliable chipless RFID humidity sensor tag based on silicon nanowires," *IEEE Trans. Microw. Theory Techn.*, vol. 64, no. 9, pp. 2977–2985, Sep. 2016, doi: 10.1109/TMTT.2016.2594229.

[20] P. Fathi, N. C. Karmakar, M. Bhattacharya, and S. Bhattacharya, "Potential chipless RFID sensors for food packaging applications: A review," *IEEE Sensors J.*, vol. 20, no. 17, pp. 9618–9636, Sep. 2020, doi: 10.1109/JSEN.2020.2991751.

[21] G. Abosamra and H. Oqaibi, "Using residual networks and cosine distance-based K-NN algorithm to recognize on-line signatures," *IEEE Access*, vol. 9, pp. 54962–54977, 2021, doi: 10.1109/ACCESS.2021.3071479.

[22] W. Xing and Y. Bei, "Medical health big data classification based on KNN classification algorithm," *IEEE Access*, vol. 8, pp. 28808–28819, 2020, doi: 10.1109/ACCESS.2019.2955754.

[23] L. M. Arjomandi, G. Khadka, Z. Xiong, and N. C. Karmakar, "Document verification: A cloud-based computing pattern recognition approach to chipless RFID," *IEEE Access*, vol. 6, pp. 78007–78015, 2018, doi: 10.1109/ACCESS.2018.2884651.

[24] K. Han and S. H. Cho, "Advanced LANDMARC with adaptive *K*-nearest algorithm for RFID location system," in *Proc. 2nd IEEE Int. Conf. Netw. Infrastruct. Digit. Content*, Sep. 2010, pp. 595–598, doi: 10.1109/ICNIDC.2010.5657852.

[25] T. Sarkar and O. Pereira, "Using the matrix pencil method to estimate the parameters of a sum of complex exponentials," *IEEE Antennas Propag. Mag.*, vol. 37, no. 1, pp. 48–55, Feb. 1995, doi: 10.1109/74.370583.

[26] M. Aminul Islam and N. Karmakar, "Design of a 16-bit ultra-low cost fully printable slot-loaded dual-polarized chipless RFID tag," in *Proc. APMC*, Melbourne, VIC, Australia, Dec. 2011, pp. 1482–1485.

[27] Y. Chareonsiri, W. Thaiwirot, and P. Akkaraekthalin, "Design of ultra-wideband tapered slot antenna by using binomial transformer with corrugation," *Frequenz*, vol. 71, nos. 5–6, pp. 251–260, Jan. 2017, doi: 10.1515/freq-2016-0131.

[28] K. Suresh, V. Jeoti, and M. Drieberg, "A read range maximization approach for UWB surface acoustic wave (SAW) RFID tags based on interdigital transducer (IDT) as a reflector," in *Proc. IEEE 6th World Forum Internet Things (WF-IoT)*, Jun. 2020, pp. 1–6, doi: 10.1109/WF-IoT48130.2020.9221414.

[29] K. Suresh, V. Jeoti, M. Drieberg, S. Soeung, A. Iqbal, G. M. Stojanovic, and S. Sarang, "Simultaneous detection of multiple surface acoustic wave sensor-tags for water quality monitoring utilizing cellular code-reuse approach," *IEEE Internet Things J.*, early access, May 21, 2021, doi: 10.1109/JIOT.2021.3082141.

FEAVEYA KHEAWPRAE (Member, IEEE) was born in Bangkok, Thailand, in 1991. She received the B.Eng. and M.Eng. degrees in electrical engineering from King Mongkut's University of Technology North Bangkok (KMUTNB), Bangkok, in 2013 and 2016, respectively, where she is currently pursuing the Ph.D. degree. Her Ph.D. degree is supported by the National Research Council of Thailand (NRCT) through the Research and Researchers for Industries (RRI). Her main research interests include chipless RFID systems, signal processing for electromagnetic applications, and radar target identification.

AKKARAT BOONPOONGA (Member, IEEE) received the B.Eng. degree in electrical engineering from King Mongkut's University of Technology North Bangkok (KMUTNB), Bangkok, Thailand, in 2002, and the M.Eng. degree in telecommunications engineering and the D.Eng. degree in electrical engineering from King Mongkut's Institute of Technology Ladkrabang (KMITL), Bangkok, in 2004 and 2008, respectively. He is currently an Associate Professor with the Department of Electrical and Computer Engineering, Faculty of Engineering, KMUTNB. His research interests include ground-penetrating radar (GPR), radar systems, radar target identification, the chipless RFID systems, and signal processing for EM applications. He is a member of ECTI Association. He was a Board Committee Member of ECTI Association, Thailand, from 2016 to 2017 and 2020 to 2021.

PRAYOOT AKKARAEKTHALIN (Member, IEEE) received the B.Eng. and M.Eng. degrees in electrical engineering from King Mongkut's University of Technology North Bangkok (KMUTNB), Bangkok, Thailand, in 1986 and 1990, respectively, and the Ph.D. degree from the University of Delaware, Newark, DE, USA, in 1998. From 1986 to 1988, he was a Research and Development Engineer with Microtek Products Company Ltd., Thailand. In 1988, he joined the Department of Electrical Engineering, KMUTNB. He was the Head of the Senior Research Scholar Project, which was supported by Thailand Research Fund, from 2015 to 2017. He has authored or coauthored more than 40 international articles, more than 200 conference papers, and four books/book chapters. His current research interests include RF/microwave circuits, wideband and multiband antennas, telecommunications, and sensor systems. He is a member of IEICE, Japan; ECTI Association, Thailand; and EEAAT Association, Thailand. He was the Chairman of IEEE MTT/AP/ED Thailand Joint Chapter, from 2007 to 2010; the Vice President of ECTI Association, from 2012 to 2013; and the President of ECTI Association, from 2014 to 2015. He was the Editor-in-Chief of *ECTI Transactions on Electrical Engineering, Electronics, and Communications*, from 2011 to 2013.

• • •